Oral presentation | Multi-phase flow
Multi-phase flow-I
Mon. Jul 15, 2024 10:45 AM - 12:45 PM Room D

# [1-D-01] Is Stokes Number Appropriate for Predicting Multiphase Richtmyer–Meshkov Instability Mixing Zone Width?

*Yingming Si[1,2], Baoqing Meng[1], Chun Wang[1], Baolin Tian[3] （1. Institute of Mechanics, Chinese Academy of Sciences, 2. University of Chinese Academy of Sciences, 3. Beihang University）

Keywords: Richtmyer–Meshkov Instability, Particle Parameters, Mixing Zone Width, Theoretical Model

©Retained by Authors

**Twelfth International Conference on Computational Fluid Dynamics (ICCFD12), Kobe, Japan, July 14-19, 2024**

# Is Stokes Number Appropriate for Predicting Multiphase Richtmyer–Meshkov Instability Mixing Zone Width?

Yingming Si[*,**], Baoqing Meng[*], Chun Wang[*], Baolin Tian[***]
Corresponding author: mengbaoqing92@foxmail.com
* Institute of Mechanics, Chinese Academy of Sciences, China
** University of Chinese Academy of Sciences, China
*** Beihang University, China

**Abstract:** Particle parameters have a significant impact on the evolution of the mixing zone width of the multiphase Richtmyer Meshkov instability (RMI), but the influence law remains to be explored. Based on the interface motion equation and integrating the influence of particle volume fraction, radius and gas viscosity parameters, this article proposes a dimensionless number *Sd* to characterize the influence of drag force on the fluid velocity relaxation process. Based on the small-perturbation theory, a growth model for the mixing zone width under extreme particle parameters is established. The analysis showed that the combination of particle density and radius determines the growth pattern of the mixing zone width. It shows exponential growth when the particle density is large, and linear growth when the radius is large or both are large. Further analysis revealed the influence of changes in particle parameters on the mixing zone width, and found that increasing the particle radius will promote the growth of the mixing zone width. Numerical simulation results verify the validity of the theoretical model and Sd number. The results indicate that the classical Stokes number (*St*) fails in predicting the growth of the mixing zone width, and the combination of *St* number and *Sd* number is the dominant dimensionless number for the evolution of multiphase RMI.

*Keywords:* Richtmyer–Meshkov Instability, Particle Parameters, Mixing Zone Width, Theoretical Model.

## 1 Introduction

The Richtmyer-Meshkov instability (RMI) phenomenon refers to the process of interface instability induced by instantaneous acceleration at the interface of two fluids of different densities[1]. This phenomenon is widely present in natural and engineering applications[2–6], such as supernova explosions[7], volcano eruption[8], inertial confinement fusion[9], and supersonic combustion[10–12]. These processes are often accompanied by dispersed phases such as particles, so it is necessary to study the multiphase RMI problem. In the process of flow instability, the "bubble" structure refers to the area where the light fluid penetrates into the heavy fluid, while the "spike" structure refers to the area where the heavy fluid penetrates into the light fluid[13]. The distance between the bubble and the spike is called the mixing zone width, which is used to characterize the degree of mixing of the two fluids. The evolution of the mixing zone width is one of the focuses of multiphase RMI research.

The dispersion of particles has an important influence on the evolution of the mixing zone width, and the density and radius of the particles are important physical parameters. In actual situations, the density and radius of particles often have a large range of variation. In this study, we used the two as coordinate axes to draw a phase diagram as shown in Figure 1, in which there are four extreme states: the density and radius of the particles are extremely small (State A), the density of the particles is extremely large and the radius is extremely small (State B), the density of the particles is extremely small and the radius is extremely large (State C), and the density and radius of the particles are extremely large (State D). By changing one of the density and radius, there are four paths for the transition between

the four states: a) increase the density when the radius is small, b) increase the radius when the density is small, c) increase the radius when the density is large, and d) increase the density when the radius is large. Thus, we construct the basis of the particle parameter phase diagram involved in this article.

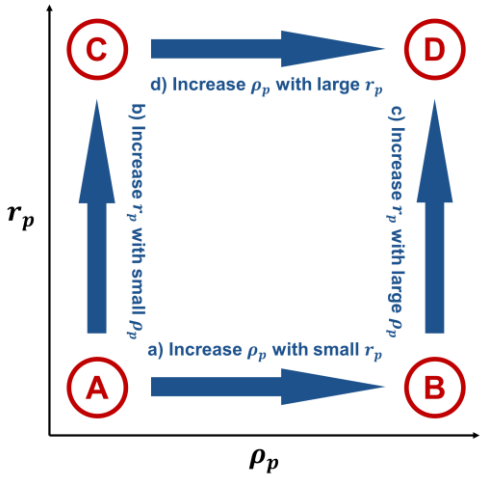


Figure 1 State phase diagram based on particle density and radius

In existing multiphase RMI related studies, particle density and radius are often combined as a dimensionless number, namely the Stokes number (*St*). The *St* number is defined as the ratio of the particle relaxation time to the flow characteristic time, as shown below:

$$St = \frac{t_p}{t_f}. \tag{1}$$

The relaxation time of a particle refers to the ratio of the particle mass to the Stokes drag coefficient, as shown below:

$$t_p = \frac{\rho_p V_p}{6\pi r_p \mu}, \tag{2}$$

where $\rho_p$, $V_p$, $r_p$ and $\mu$ are the particle density, volume, radius and fluid dynamic viscosity respectively. The flow characteristic time varies from problem to problem. In this study, it is defined as the ratio of the wavelength of the interface disturbance to the velocity of the interface after being accelerated by the shock wave, as shown below:

$$t_f = \frac{\lambda}{U^+_{inf0}}. \tag{3}$$

The *St* number measures the ability of particles to follow the fluid: a small *St* value ($St \ll 1$) indicates that the particle velocity can quickly reach equilibrium with the fluid velocity, while a large *St* value ($St \gg 1$) indicates that it is difficult for the particle velocity to reach equilibrium with the fluid velocity. The *St* number is an important parameter for multiphase RMI flows containing particles, reflecting the combined effects of particle density and radius.

In the existing research, for State A, previous research work has been carried out on gas-particle flow with small St number. Through theoretical derivation and numerical verification, the linear growth model of the mixing zone width was given[13–16]. In 1961, Saffman et al.[14] established a governing equation to describe the motion of gas carrying small dust particles. In 2010, Ukai et al.[13] performed small perturbation analysis and derived a linear theoretical solution to the growth rate of the mixing zone width of sparse gas-particle flow with a small *St* number, and gave the multiphase Atwood number to describe the density difference of multiphase fluids on both sides of the interface. Since then, some scholars have extended the model to nonlinear stages or dense flow conditions[16–18], which all reflect the influence of air-particle coupling. Different from the pure gas phase RMI problem[19–21], the multiphase RMI problem is affected by particle parameters, the complexity of the flow system is higher than that of the classical RMI, and the corresponding theoretical model and evolution mechanism are not yet mature.

Therefore, numerical simulation is often used to study the impact of particles. The *St* number is closely related to the relaxation time of particles and has also received close attention. Ukai et al.[13] carried out numerical simulations on dilute gas-particle flows with large *St* numbers and found that large-sized particles do not follow the movement of the fluid, and the growth rate of the mixing zone width has nothing to do with the particles, which is consistent with the growth model of the pure gas phase RMI. McFarland et al.[22] also conducted detailed numerical simulation studies on the influence of particle relaxation time. They controlled the relaxation time by changing the particle radius and showed that larger particles slow down the entire interface as they propagate downstream, resulting in a significant attenuation of the mixing zone width. They also pointed out that for small relaxation time, the multiphase Atwood number proposed by Ukai et al.[13] is effective in predicting the evolution of the mixing zone width; but for large relaxation time, the growth of the mixing zone width is close to the classical pure gas phase RMI model.

According to the simulation results of this study, *St* is not the only dominant dimensionless number of the evolution of multiphase RMI, and the growth of the mixing zone width cannot be accurately predicted by the *St* number. For flows with the same *St* number, different combinations of particle density and radius may lead to completely different evolutions of the mixing zone width. The potential dominant dimensionless number of this process remains to be studied, the theoretical model of the growth of the mixing zone width under different conditions needs to be improved, and the influence of particle parameter transitions between different states on the mixing zone width also needs to be explored.

Based on the phase diagram composed of particle density and radius, this article studies the theoretical model of the mixing zone width of the multiphase RMI under extreme conditions and the transformation law between them. We combined the parameters such as particle volume fraction, radius and gas viscosity, and proposed a new dimensionless number *Sd* number, which can more effectively predict the growth law of the mixing zone width than the *St* number. On this basis, a theoretical model of the growth rate under the extreme state was established, which complemented the analytical solution in the phase diagram. Combining theoretical analysis and Compressible-Multi-Phase Particle-in-Cell method (CMP-PIC)[23,24], the transformation law between different extreme states in the phase diagram was revealed, and the correctness and effectiveness of the theoretical model and *Sd* number were verified.

# 2 Dimensionless Number and Multiphase RMI Theoretical Model

Based on the interface motion control equation, we derived a new dimensionless number *Sd* number. Based on the *Sd* number, we established a theoretical model for the B, C, and D states in the phase diagram.

## 2.1 Dimensionless Number to Measure the Drag Coupling Effect

The growth of the mixing zone width is closely related to the interface motion speed. Therefore, we start from the momentum equation and derive the fluid motion control equation near the interface based on the Lagrangian perspective[17], which is as follows:

$$\alpha_f \rho_f \frac{DU_{inf}}{Dt'} = -\frac{\alpha_p}{V_p}\kappa\left(U_{inf} - v_{px}\right) - \alpha_f \frac{\partial P_f}{\partial x}, \tag{4}$$

where $\alpha_f$ is the volume fraction of the fluid, $\rho_f$ is the density of the fluid, $U_{inf}$ is the velocity of the interface, $t' = t - t_0^+$, $t_0^+$ is the moment when the shock wave passes through the interface, $\alpha_p$ is the volume fraction of the particle, $v_{px}$ is the velocity of the particle in the direction of fluid motion, and $P_f$ is the fluid pressure. The left side of the equation is the inertia term of the fluid near the interface, and the right side represents the momentum source term, named the drag term and the pressure gradient

term.

Without changing the fluid type and Mach number, the *St* number is only related to the particle radius and density, that is $St \propto \rho_p r_p^2$. Therefore, the *St* number is usually changed by the particle density or radius. In the drag term of equation (4), increasing the particle density will lead to a decrease in particle velocity, an increase in the velocity difference between the phases, and thus an increase in the absolute value of the drag, which will reduce the fluid velocity at the interface; while increasing the particle radius will lead to an increase in the particle volume, which means a decrease in the number of particles when the particle volume fraction remains unchanged, thus reducing the absolute value of the drag and increasing the fluid velocity at the interface. Figure 2 shows the impact of the two paths of increasing the *St* value. It can be seen that even if *St* increases to the same extent, changing different particle parameters will cause the fluid velocity to develop in different directions. This is also the main reason why the growth of the mixing zone width cannot be accurately predicted based on the *St* number. Therefore, a new dimensionless number is needed to measure the drag force.

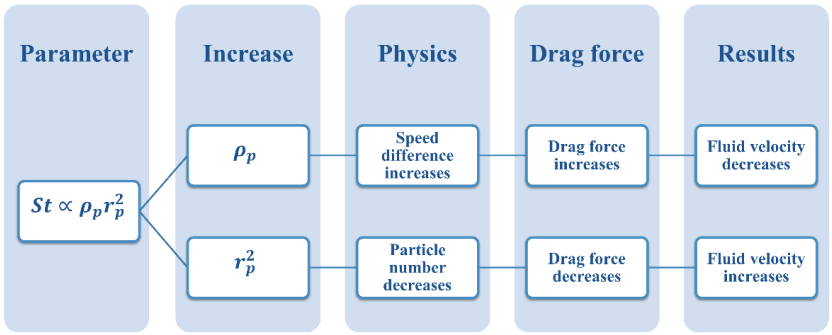


Figure 2 Two paths of different fluid velocity changes caused by increasing particle density or radius

The drag force has an important influence on the fluid velocity, so we first consider the interface motion equation with only the drag force acting on it:

$$\alpha_f \rho_f \frac{DU_{inf}}{Dt'} = -\frac{\alpha_p}{V_p}\kappa\left(U_{inf} - v_{px}\right). \tag{5}$$

When the *St* number is large, the particle velocity does not change significantly. Considering when $t' = 0$, $U_{inf} = U_{inf0}^{+}$. Integrating the above equation yields the following equation:

$$U_{inf} = \left(U_{inf0}^{+} - v_{px}\right)e^{-t'/t_{drag}} + v_{px}, \tag{6}$$

where the dimension of $t_{drag}$ is time, and its expression is as follows:

$$t_{drag} = \frac{\alpha_f \rho_f V_p}{\alpha_p \kappa}, \tag{7}$$

which represents the characteristic time when drag force has a significant effect on fluid velocity. Therefore, we define the ratio of the relaxation time of fluid affected by drag force to the flow characteristic time as a new dimensionless number *Sd* to measure the influence of drag force on fluid velocity[25]. The specific expression of the *Sd* number is:

$$Sd = \frac{t_{drag}}{t_f} = \frac{\alpha_f}{\alpha_p}\frac{\rho_f V_p U_{inf0}}{\kappa\lambda}. \tag{8}$$

The *Sd* number is determined by both the fluid and the particles. The parameters $\alpha_p$, $V_p$, $\kappa$ and are usually variable, so this dimensionless number is closely related to the particle volume fraction $\alpha_p$, the particle radius $r_p$, and the gas dynamic viscosity $\mu$. When $Sd \ll 1$, the relaxation time of the drag force affecting the fluid motion is much smaller than the flow characteristic time, the drag force can change the fluid velocity more quickly during the process; on the contrary, when $Sd \gg 1$, the drag force can hardly affect the fluid velocity.

*Sd* numbers have different properties from *St* numbers. From equation (8), The expression of *Sd* number includes the fluid density and the volume fraction of particles and fluid, which is different from

*St* number. From a physical perspective, the *St* number represents the effect of drag force on particle velocity, while the *Sd* number represents the effect of drag force on fluid velocity, taking into account the effect of dense particle. When the *St* number is small, the particles can quickly catch up with the fluid, and the velocity difference between the phases is extremely small, resulting in an insignificant drag effect on the fluid, and the *Sd* number to measure the drag force is useless in this case, corresponding to the State A in the phase diagram. When the *St* number is large, the lag in the particle velocity will lead to an obvious speed difference, and the *Sd* number comprehensively considers physical parameters to measure the drag force, thereby judging the evolution trend of the fluid velocity and the mixing zone width, corresponding to the States B, C and D in the phase diagram.

## 2.2 Growth Model of the Mixing Zone Width in the Phase Diagram.

Due to the complexity of multiphase RMI flow, it is difficult to construct a growth model of the mixing zone width for each point in the phase diagram. We only consider the case of extremely particle density or radius to simplify the analysis process. The theoretical growth model of the mixing zone width under the extreme State A has been given by predecessors[13,16]. Here we use the dimensionless number *Sd* as the flow state division standard and give the growth model of the mixing zone width under the Extreme States B, C, and D.

For State B where the particle density is large and the radius is small, the *Sd* number is relatively small, and the drag force dominates the gas velocity, so the pressure gradient term is smaller than the drag term. In addition, due to the large *St* number, the particle gradually accelerates slowly from rest, thus $v_{px} \ll U_{inf}$. The interface motion equation can be simplified to:

$$\alpha_f \rho_f \frac{DU_{inf}}{Dt'} = -\frac{\alpha_p \kappa}{V_p} U_{inf}. \tag{9}$$

At the moment when the shock wave passes through the interface, the velocity of the interface is $U_{inf0}^{+}$, and the solution of equation (9) is:

$$U_{inf} = U_{inf0}^{+} e^{-\frac{\alpha_p \kappa}{\alpha_f \rho_f V_p} t'}, \tag{10}$$

According to previous small-perturbation theory research, the amplitude of the perturbation in the RMI problem has the following relationship with the interface motion velocity and the multiphase Atwood number[1,13]:

$$\frac{da}{dt} = k a_0^{+} A_m U_{inf}, \tag{11}$$

where $k$ is the wave number of the interface disturbance and $a_0^{+}$ is the disturbance amplitude after the shock wave passes. $A_m = \frac{\rho_2 - \rho_1}{\rho_2 + \rho_1}$ can describe the difference in gas density before and after the interface. The value of the mixing zone width $h$ is twice the disturbance amplitude. Therefore, we get the growth rate of the mixing zone width as follows:

$$\frac{dh}{dt} = 2k a_0^{+} A_m U_{inf0}^{+} e^{-t'/t_{drag}}. \tag{12}$$

By integrating the growth rate, we obtain the growth model of the mixing zone width under the conditions of large particle density and small radius, as shown below:

$$h = -2k a_0^{+} A_m U_{inf0}^{+} t_{drag} \left(e^{-t'/t_{drag}} - 1\right) + h_0^{+}, \tag{13}$$

where $h_0^{+}$ is the value of the mixing zone width when the shock wave passes through the interface. This equation is in exponential form and does not include the particle density $\rho_p$, so the mixing zone width in this model is only related to the particle radius and has nothing to do with the particle density.

For State C where the particle density is small and the radius is large, the *Sd* number is relatively large and the drag term is approximately zero. The interface motion equation can be simplified to:

$$\alpha_f \rho_f \frac{DU_{inf}}{Dt'} = -\alpha_f \frac{\partial P_f}{\partial x}, \tag{14}$$

The above equation does not contain any particle-related parameters and is the same as the classic pure gas phase RMI problem equation. Therefore, its solution should be equivalent to the linear form solution of the gas phase RMI problem, as shown below:

$$\frac{dh}{dt} = 2ka_0^+ A_m U_{inf0}^+. \tag{15}$$

By integrating the growth rate, we obtain the growth model of the mixing zone width under the conditions of large particle radius and small density, as shown below:

$$h = 2ka_0^+ A_m U_{inf0}^+ t' + h_0^+. \tag{16}$$

The equation is in linear form, the same as the pure gas phase RMI problem. Therefore, the mixing zone width in this model is independent of the particle density and radius.

For State D with large particle density and large radius, the *Sd* number is also relatively large. The theoretical solution under large *Sd* number is independent of particle density, so the theoretical solution of State D is the same as that of State C, both of which have theoretical solutions with linear form, i.e., equation (16). In addition, State D can be regarded as adding the extreme large particle radius condition on the basis of State B, or as adding the extreme large particle density condition on the basis of State C. The expression of equation (13) in the case of limit particle radius is the same as that of equation (16) in the case of maximum particle density, which also proves the consistency and unity of the theoretical model. It should be noted that the above theoretical solution is still based on small-perturbation theory and is only applicable to the early evolution of the shock-driven interface under low Mach number.

In this section, we combine the effects of particle volume fraction, radius, and gas viscosity, and derive a dimensionless number to characterize the effect of drag on gas velocity based on the ratio of drag relaxation time to flow characteristic time. Based on the small-perturbation theory, a theoretical model of the growth rate of the mixing zone width at the extreme particle density and radius is established. When the particle density is large, the mixing zone width increases exponentially with time, and when the particle radius is large or both are large, the mixing zone width increases linearly with time, completing the theoretical solutions at each extreme state in the particle parameter phase diagram.

# 3 Multiphase RMI Numerical Simulation and Phase Diagram Analysis

We set up a series of cases to simulate the evolution of the mixing zone width of multiphase RMI by changing the density and radius of the particles. The evolution trend and relative change of the mixing zone width are predicted based on the theoretical model. By comparing and analyzing the results of the numerical simulation, we summarized the influence of particle parameters on the evolution of multiphase RMI and verified the correctness and effectiveness of the multiphase RMI theoretical model.

## 3.1 Numerical Methods and Mesh Independence Verification

We use the CMP-PIC method based on the Euler-Lagrangian framework to simulate multiphase flow[23,24], which can simulate the all pattern flows from dilute to dense and granular flow. The Runge–Kutta method is used for time advancement, the TVD format[26] is used to reconstruct the flow variables, and the Riemannian solver proposed by Harten et al.[27] is applied to solve the flux. Particles with similar physical properties are packaged into parcels, and the soft ball model is used to calculate collisions between particles, which facilitates the calculation of interphase coupling and significantly reduces the amount of calculations required for large-scale particle group simulations. The CMP-PIC method is widely used in the simulation of shock-particle group interaction and multiphase RMI, and has achieved good application results. For verification of this method, please refer to published papers[16,17,23,28,29].

We carried out mesh-independence verification and used four different mesh resolutions to check

the convergence of the results. Detailed data are listed in Table 1. Other conditions are set in the same way as Case1 in Section 3.2. *Nx* and *Ny* are the number of meshs in the *x* and *y* directions respectively. The curve of the mixing zone width changing with time is shown in Figure 3. The results of Resolution C and Resolution D are in good agreement, indicating that further refinement of the mesh has no significant impact on the simulation results. Considering the calculation time, subsequent calculation cases use Resolution C to carry out simulations. In addition, according to the research of Ukai and Meng et al.[13,16,23], arranging four particle packets in each mesh unit can ensure the convergence of the particle packet resolution within the mesh.

Table 1 Detailed information on four mesh resolutions

| Case | *Nx* | *Ny* | Mesh Number | Parcel Number |
|---|---|---|---|---|
| Resolution A | 300 | 50 | 15 000 | 45 000 |
| Resolution B | 600 | 100 | 60 000 | 180 000 |
| Resolution C | 1200 | 200 | 240 000 | 720 000 |
| Resolution D | 1800 | 300 | 540 000 | 1620 0000 |

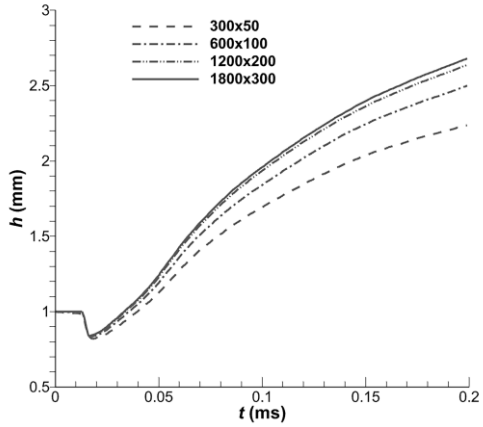


Figure 3 Mixing zone widths of four resolutions

## 3.2 Multiphase RMI Simulation Case Setup

The shock wave with *Ma*=1.2 passes through the two-dimensional cosine-shaped single-mode air/SF6 interface, and particles with uniform diameter and density are uniformly distributed in space[28], as shown in Figure 4. Among them, the light fluid is air, the heavy fluid is SF6, and the yellow dots represent parcels. A cosine-shaped perturbation is added to the interface, as shown in equation (17), where $a_0$ is the initial interface amplitude and $\lambda$ is the initial interface wavelength. The similar calculation domain settings can refer to existing studies[16–18,22]. The position of the interface is defined as the position where the air volume fraction $\beta_1 = 0.5$. The volume fraction of air in the gas phase is smoothed around the interface using an error function[30].

$$a(y) = a_0 \cos\left(\frac{2\pi}{\lambda} y\right). \tag{17}$$

Table 2 lists other initial condition parameters required for the calculation, where $L_x$ is the flow length of the calculation domain, $L_y$ is the longitudinal length of the calculation domain, $L_{shock}$ is the initial shock wave position, $L_{interface}$ is the initial position of the air/SF6 interface, $L_{particle}$ is the initial position of the particle distribution, $P_0$ is the shock-free fluid pressure, and $\alpha_{p0}$ is the initial volume fraction of the particles. The left boundary of the calculation domain is set as the airflow inlet condition, the right boundary is set as the airflow outlet condition, and the upper and lower sides of the domain are set as periodic boundaries of gas and particles.

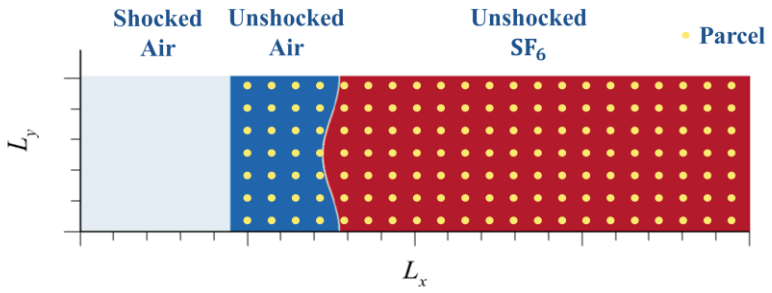


Figure 4 Schematic diagram of multiphase RMI calculation with uniformly distributed particles

Table 2 Calculation domain settings and flow field initial conditions

| $L_x$ | $L_y$ | $L_{shock}$ | $L_{interface}$ | $L_{particle}$ | $a_0$ | $\lambda$ | $P_0$ | $Ma$ | $\alpha_{p0}$ |
|---|---|---|---|---|---|---|---|---|---|
| 60mm | 10mm | 9mm | 15mm | >10mm | 0.5mm | 10mm | 101kPa | 1.2 | 1% |

Considering that the *St* number is related to the particle density and radius, while the *Sd* number is only related to the particle radius, we change the particle density and radius to make the *St* number and *Sd* number change regularly, set up a series of cases to simulate the multiphase RMI problem, and explore the influence of particle parameters on the mixing zone width. Table 3 lists the detailed information of each case. In Case 1, the particle density $\rho_{p,1} = 500\text{kg/m}^3$, the particle radius $r_{p,1} = 5\mu\text{m}$, the *St* number is about 1, and the *Sd* number is about 0.2. Case 1 is used as the benchmark case, and the particle density and radius of the remaining cases are dimensionless, that is, $\hat{\rho}_p = \rho_p/\rho_{p,1}$, $\hat{r}_p = r_p/r_{p,1}$.

Table 3 Particle parameters and corresponding dimensionless numbers under different cases

| Case | $\hat{\rho}_p$ | $\hat{r}_p$ | $St$ | $Sd$ |
|---|---|---|---|---|
| 1 | 1 | 1 | $\approx 10^0$ | ≈0.2 |
| 2 | 9 | 1 | $\approx 10^1$ | ≈0.2 |
| 3 | 100 | 1 | $\approx 10^2$ | ≈0.2 |
| 4 | 900 | 1 | $\approx 10^3$ | ≈0.2 |
| 5 | 1 | 3 | $\approx 10^1$ | ≈2 |
| 6 | 1 | 10 | $\approx 10^2$ | ≈20 |
| 7 | 1 | 30 | $\approx 10^3$ | ≈200 |
| 8 | 900 | 3 | $\approx 10^4$ | ≈2 |
| 9 | 900 | 10 | $\approx 10^5$ | ≈20 |
| 10 | 900 | 30 | $\approx 10^6$ | ≈200 |
| 11 | 9 | 30 | $\approx 10^4$ | ≈200 |
| 12 | 100 | 30 | $\approx 10^5$ | ≈200 |

In order to show the relationship between different cases more clearly, we plot them on a phase diagram consisting of particle density and radius, as shown in Figure 5. The horizontal and vertical axes in the figure are logarithmic scales. A, B, C, and D are the four states of extreme particle density and radius defined in the Figure 1. With them as endpoints, there are four paths for changing a single parameter. The series of cases are set along these four paths to compare, analyze, and explore the changing rules between different states.

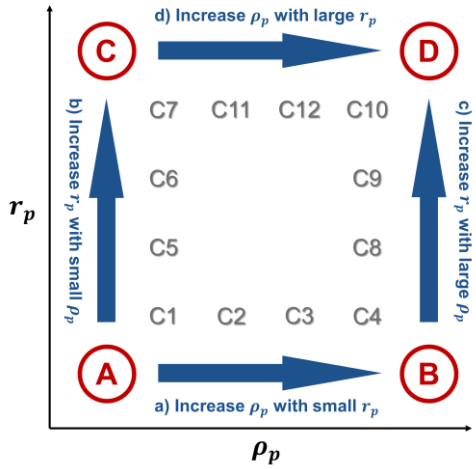


Figure 5 Distribution of the calculation cases on phase diagram based on particle density and radius

## 3.3 Variation of the Mixing Zone Width Between Different Extreme States

Based on the theoretical model in Section 2, we predict the variation of the mixing zone width for different cases on Paths a), b), c), and d) in the phase diagram, and verify it with the results obtained from numerical simulation:

a): Under the condition of small particle radius, the particle density is gradually increased. For Cases 1, 2, 3, and 4, the dimensionless particle density is 1, 9, 100, and 900, respectively. According to the theoretical model analysis, as the particle density gradually increases, the *St* number gradually increases, while the *Sd* number remains unchanged. The particle movement speed slows down, which increases the velocity difference between phases, resulting in an increase in drag and thus reducing the mixing zone width. In addition, when the particle density is large enough, the mixing zone width should gradually approach the theoretical solution of the exponential form under State B. The numerical simulation results of the mixing zone width of Cases 1, 2, 3, and 4 are shown in Figure 6. Within the given calculation time (0.2ms), the mixing zone width increases with time after the shock wave passes. From Cases 1 to 4, the particle density increases, and the mixing zone width decreases, and finally approaches the theoretical solution of the exponential form.

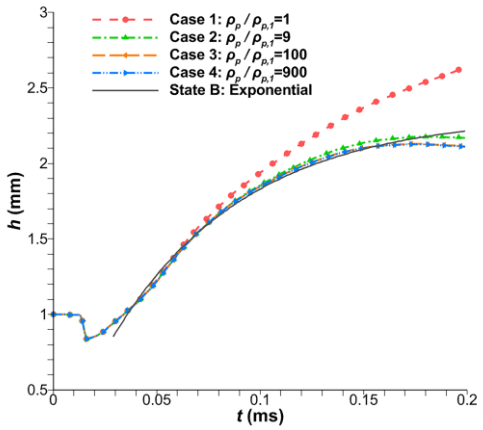


Figure 6 Mixing zone width evolutions with small particle radius and increasing particle density

b): Under the condition of small particle density, the particle radius is gradually increased. For Cases 1, 5, 6, and 7, the dimensionless particle radius is 1, 3, 10, and 30, respectively. According to the theoretical model analysis, as the particle radius gradually increases, the *St* number and the *Sd* number gradually increase. When the volume fraction remains unchanged, the increase in particle volume is

equivalent to the decrease in the number of particles, resulting in a decrease of the drag force, thereby increasing the mixing zone width. In addition, when the particle radius is large enough, the mixing zone width should gradually approach the theoretical solution of the linear form under State C. The numerical simulation results of the mixing zone width of Cases 1, 5, 6, and 7 are shown in Figure 7. Within 0.2 ms, the mixing zone width increases with time after the shock wave passes. From Cases 1 to 7, the particle radius increases, and the mixing zone width increases, and finally approaches the theoretical solution of the linear form.

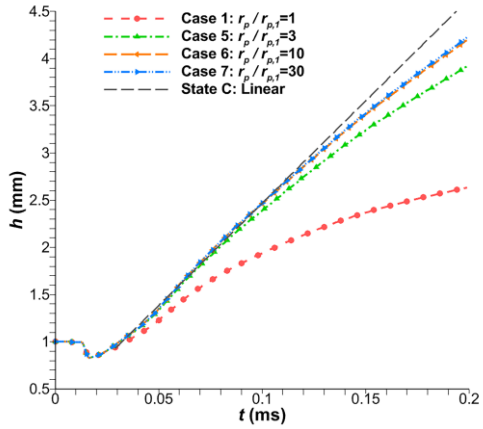


Figure 7 Mixing zone width evolutions with small particle density and increasing particle radius

c): Under the condition of large particle density, the particle radius gradually increases. For Cases 4, 8, 9, and 10, the dimensionless particle radius is 1, 3, 10, and 30, respectively. According to the theoretical model analysis, as the particle radius gradually increases, *St* and *Sd* gradually increase, and the drag force gradually weakens, resulting in an increase in the mixing zone width. Since the particle density is large enough, the four curves should all be exponential and only related to the particle radius. As the radius increases, the mixing zone width gradually changes from the exponential form under State B to the linear form under State D. The numerical simulation results of the mixing zone width of Cases 4, 8, 9, and 10 are shown in Figure 8. Within 0.2ms, the mixing zone width increases with time after the shock wave passes. From Cases 4 to 10, the particle radius increases, and the mixing zone width increases, gradually evolving from an exponential solution to a linear solution.

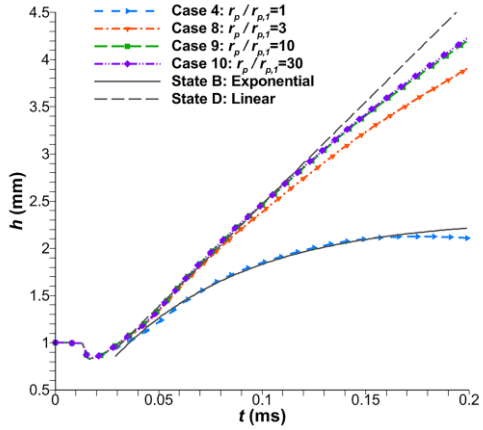


Figure 8 Mixing zone width evolutions with large particle density and increasing particle radius

d): Under the condition of large particle radius, the particle density is gradually increased. For Cases 7, 11, 12, and 10, the dimensionless particle density is 1, 9, 100, and 900, respectively. According to the theoretical model analysis, as the particle density gradually increases, the *St* number gradually increases, while the *Sd* number remains unchanged. However, the particles in the four cases have almost remained stationary, and the drag force no longer changes, so the mixing zone width curves almost

overlap. Since the particle radius is large enough, the four curves all degenerate into linear forms, which are independent of the particle density and radius. Therefore, the mixing zone width always maintains the linear form under state C or D. The numerical simulation results of the mixing zone width of Cases 7, 11, 12, and 10 are shown in Figure 9. Within 0.2ms, the mixing zone width increases with time after the shock wave passes. From Cases 7 to 10, the particle density increases, and the mixing zone width remains unchanged, which is always consistent with the linear theoretical solution.

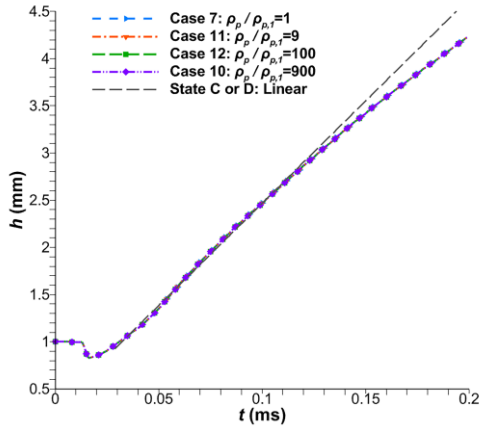


Figure 9 Mixing zone width evolutions with large particle radius and increasing particle density

Combining the cases on the four paths, we can see that the results of the numerical simulation are consistent with the predictions of the theoretical analysis. In addition, we summarize the influence of particle parameters on the mixing zone width: increasing the particle radius will increase the mixing zone width. In general, the mixing zone width increases with the increase of the *Sd* number.

Furthermore, we discuss the situation where the *St* number gradually increases to illustrate the failure of the *St* number in predicting the growth of the mixing zone width. Taking State A as the starting position and State D as the ending position, two long parameter change paths are planned: Path 1 is State A→B→D, corresponding to Case 1→2→3→4→8→9→10, and Path 2 is State A→C→D, corresponding to Case 1→5→6→7→11→12→10. On each path, the *St* numbers of adjacent cases differ by about 10 times, and the *St* numbers of the corresponding cases on the two paths are equal in turn. The mixing zone width at 0.2ms on the two paths is plotted as shown in Figure 10.

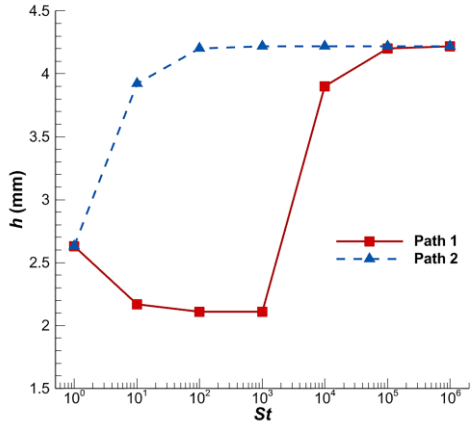


Figure 10 Bifurcation of mixing zone widths with St number on two paths at 0.2 ms

It can be seen from Figure 10 that for the same starting and ending positions, gradually increasing the *St* number and adopting different particle parameter change paths will cause the mixing zone width to bifurcate: in Path 1, first increasing the particle density and then increasing the particle radius will cause the mixing zone width to experience a process of first decreasing and then increasing, while in

Path 2, first increasing the particle radius and then increasing the particle density will cause the mixing zone width to experience a process of first increasing and then remaining unchanged. The difference between the two paths shows that the *St* number fails to predict the growth of the mixing zone width. There is no obvious monotonic relationship between the mixing zone width and the *St* number, and its evolution depends on the specific changes in particle density and radius. This also reflects the complexity of the influence of particle parameters on the evolution of the mixing zone width.

## 3.4 Validation of Dimensionless Numbers Sd

Considering the *Sd* number and the theoretical models of the mixing zone width do not contain the particle density, the mixing zone width is independent of the particle density. Without changing the gas parameters, the *Sd* number and the particle radius are equivalent. Therefore, for cases with the same *Sd* number and different *St* number, their mixing zone widths should also be similar.

We set four groups of cases with different *St* numbers and the same *Sd* number. Group A includes Cases 1, 2, 3, and 4, whose *Sd* numbers are about 0.2; Group B includes Cases 5 and 8, whose *Sd* numbers are about 2; Group C includes Cases 6 and 9, whose *Sd* numbers are about 20; Group D includes Cases 7, 11, 12, and 10, whose *Sd* numbers are about 200. The mixing zone width curves of each group are plotted and compared, as shown in Figure 11.

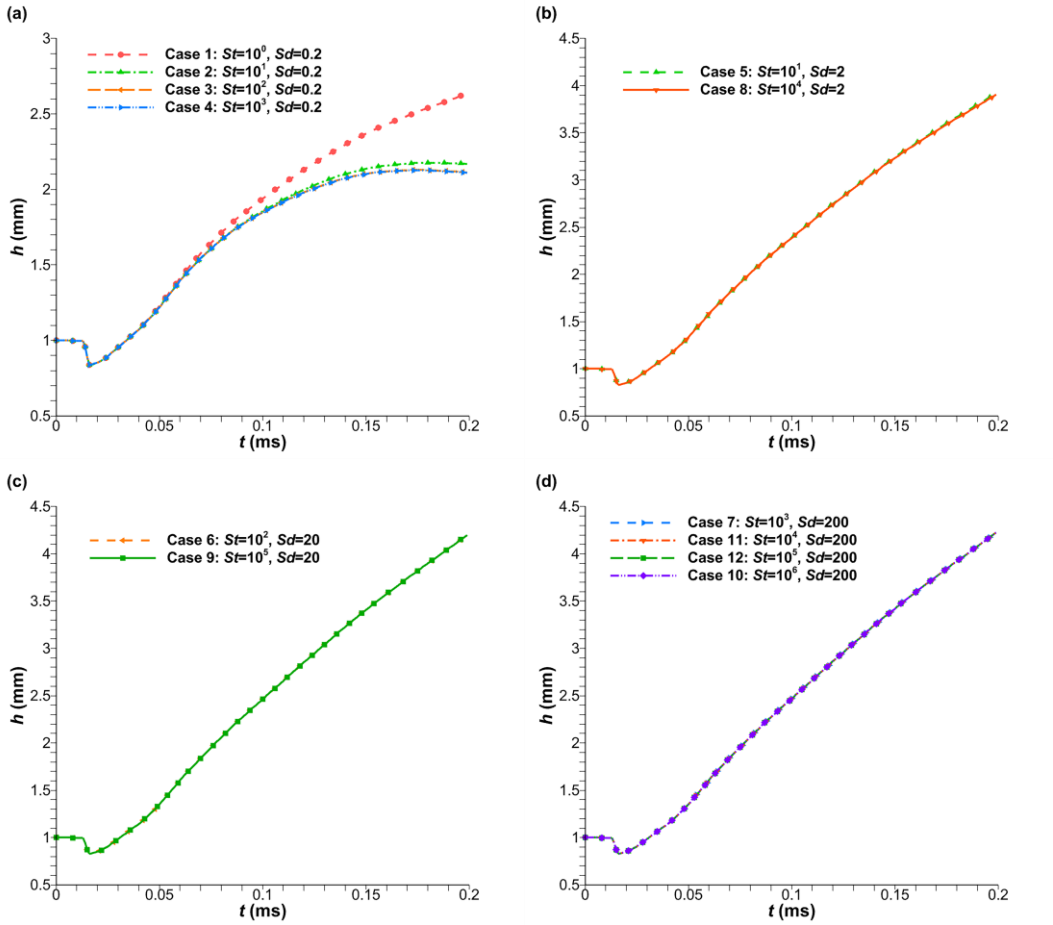


Figure 11 Comparison of mixing zone widths for calculation cases with the same *Sd* number. (a) *Sd*≈0.2; (b) *Sd*≈2; (c) *Sd*≈20; (d) *Sd*≈200

For the cases in group A with a small *St* number, as the particle density increases, the particle velocity changes from closely following the fluid movement to gradually lagging behind until it is almost stationary. Therefore, although the cases in group A have the same *Sd* number, the mixing zone width curves are not completely consistent. This also indirectly shows that the *Sd* number can only

function in the case with a large *St* number. For the three Groups B, C, and D with large St numbers, the cases in each group have the same *Sd* number, and the evolution trends of their mixing zone widths are similar. This shows that in the case of a large *St* number, the *Sd* number can effectively control the multiphase RMI flow state, and further verifies the correctness of the theoretical model. For the entire phase diagram, the combination of the *St* number and the *Sd* number is the dominant parameter for the evolution of the mixing zone width.

In this section, we set up a series of cases by changing the particle parameters to simulate the evolution of the mixing zone width in multiphase RMI, and explained the influence of particle parameters in the phase diagram. The mixing zone width increases with the increase of the particle radius or *Sd* number. However, the *St* number fails in predicting the growth of the mixing zone width, and for the same starting and ending positions in the phase diagram, increasing the *St* number through different particle parameter change paths will cause a bifurcation phenomenon in the growth of the mixing zone width. For the case with a large *St* number, the *Sd* number can effectively control the evolution of the mixing zone width; and for any particle parameter conditions, the combination of the *St* number and the *Sd* number is the dominant parameter for the evolution of the mixing zone width.

# 4 Conclusion

Based on the phase diagram composed of particle density and radius, this article establishes a theoretical model for the evolution of multiphase RMI under the extreme particle density or radius, and reveals the influence of particle parameters on the mixing zone width.

Based on the momentum equation of fluid motion at the interface, we consider the influence of parameters such as particle volume fraction, radius and gas viscosity, and propose a new dimensionless *Sd*, which represents the ratio of drag relaxation time to flow characteristic time, and can effectively characterize the influence of drag on fluid velocity. Based on the small-perturbation theory, a theoretical model for the growth rate of the mixing zone width under the extreme particle density and radius is established. When the particle density is extremely large, the mixing zone width grows exponentially, and when the particle radius is extremely large or both are large, it grows linearly, completing the theoretical solutions in the phase diagram.

We carried out numerical simulations of a series of multiphase RMI problems and compared their results with theoretical predictions, revealing the influence of particle parameter changes. The mixing zone width increases with the increase of the particle radius or Sd number. In addition, *St* number fails in predicting the growth of the mixing zone width, and increasing the *St* number through different particle parameter change paths will cause a bifurcation phenomenon in the growth of the mixing zone width. For the case with large *St* number, *Sd* number can effectively control the evolution of the mixing zone width; and for any particle parameter conditions, the combination of *St* number and *Sd* number is the dominant parameter of the evolution of the mixing zone width.

The *Sd* number proposed in this article can provide support for the simulation and prediction of the evolution of multiphase RMI in the future. By changing the particle parameters to change the *Sd* number, the growth morphology of the mixing zone width can be controlled, providing new ideas for the control of multiphase RMI in practical problems.

# References

[1] Richtmyer R D. Taylor instability in shock acceleration of compressible fluids[J]. Communications on Pure and Applied Mathematics, 1960, 13(2): 297–319.

[2] Luo X, Wang M, Si T, Zhai Z. On the interaction of a planar shock with an SF6 polygon[J]. Journal of Fluid Mechanics, 2015, 773: 366–394.

[3] Luo X, Guan B, Zhai Z, Si T. Principal curvature effects on the early evolution of three-dimensional single-mode Richtmyer-Meshkov instabilities[J]. Physical Review E, 2016, 93(2): 023110.
[4] Sun R, Ding J, Zhai Z, Si T, Luo X. Convergent Richtmyer–Meshkov instability of heavy gas layer with perturbed inner surface[J]. Journal of Fluid Mechanics, 2020, 902: A3.
[5] Zhou Y, Cabot W H, Thornber B. Asymptotic behavior of the mixed mass in Rayleigh–Taylor and Richtmyer–Meshkov instability induced flows[J]. Physics of Plasmas, 2016, 23(5): 052712.
[6] Li H, He Z, Zhang Y, Tian B. On the role of rarefaction/compression waves in Richtmyer-Meshkov instability with reshock[J]. Physics of Fluids, 2019, 31(5): 054102.
[7] Sano T, Tamatani S, Matsuo K, Law K F F, Morita T, Egashira S, Ota M, Kumar R, Shimogawara H, Hara Y, Lee S, Sakata S, Rigon G, Michel T, Mabey P, Albertazzi B, Koenig M, Casner A, Shigemori K, Fujioka S, Murakami M, Sakawa Y. Laser astrophysics experiment on the amplification of magnetic fields by shock-induced interfacial instabilities[J]. Physical Review E, 2021, 104(3): 035206.
[8] Reese D T, Ames A M, Noble C D, Oakley J G, Rothamer D A, Bonazza R. Simultaneous direct measurements of concentration and velocity in the Richtmyer–Meshkov instability[J]. Journal of Fluid Mechanics, 2018, 849: 541–575.
[9] Wang L, Ye W, He X, Wu J, Fan Z, Xue C, Guo H, Miao W, Yuan Y, Dong J, Jia G, Zhang J, Li Y, Liu J, Wang M, Ding Y, Zhang W. Theoretical and simulation research of hydrodynamic instabilities in inertial-confinement fusion implosions[J]. Science China Physics, Mechanics & Astronomy, 2017, 60(5): 055201.
[10] Yang J, Kubota T, Zukoski E E. Applications of shock-induced mixing to supersonic combustion[J]. AIAA Journal, 1993, 31(5): 854–862.
[11] Bambauer M, Hasslberger J, Klein M. Direct numerical simulation of the Richtmyer–Meshkov instability in reactive and nonreactive flows[J]. Combustion Science and Technology, 2020, 192(11): 2010–2027.
[12] Fan E, Hao J, Guan B, Wen C, Shi L. Numerical investigation on reacting shock-bubble interaction at a low Mach limit[J]. Combustion and Flame, 2022, 241: 112085.
[13] Ukai S, Balakrishnan K, Menon S. On Richtmyer–Meshkov instability in dilute gas-particle mixtures[J]. Physics of Fluids, 2010, 22(10): 104103.
[14] Saffman P G. On the stability of laminar flow of a dusty gas[J]. Journal of Fluid Mechanics, 1962, 13(1): 120–128.
[15] Balakrishnan K, Menon S. A multiphase buoyancy-drag model for the study of Rayleigh-Taylor and Richtmyer-Meshkov instabilities in dusty gases[J]. Laser and Particle Beams, 2011, 29(2): 201–217.
[16] Meng B, Zeng J, Tian B, Li L, He Z, Guo X. Modeling and verification of the Richtmyer–Meshkov instability linear growth rate of the dense gas-particle flow[J]. Physics of Fluids, 2019, 31(7): 074102.
[17] Meng B, Zeng J, Tian B, Zhou R, Shen W. Modeling and simulation of a single-mode multiphase Richtmyer-Meshkov instability with a large Stokes number[J]. AIP ADVANCES, 2019, 9(12).
[18] Zheng H, Chen Q, Meng B, Zeng J, Tian B. On the nonlinear growth of multiphase Richtmyer–Meshkov instability in dilute gas-particles flow[J]. Chinese Physics Letters, 2020, 37(1): 015201.
[19] Zhou Z, Ding J, Zhai Z, Cheng W, Luo X. Mode coupling in converging Richtmyer–Meshkov instability of dual-mode interface[J]. Acta Mechanica Sinica, 2020, 36(2): 356–366.
[20] Zhang Y, Zhou Z, Ding J, Luo X. Interaction of a planar shock wave with two heavy/light interfaces[J]. Acta Mechanica Sinica, 2022, 38(9): 322047.
[21] Zhai Z, Zou L, Wu Q, Luo X. Review of experimental Richtmyer–Meshkov instability in shock tube: From simple to complex[J]. Proceedings of the Institution of Mechanical Engineers, Part C: Journal of Mechanical Engineering Science, 2018, 232(16): 2830–2849.
[22] McFarland J A, Black W J, Dahal J, Morgan B E. Computational study of the shock driven instability of a multiphase particle-gas system[J]. Physics of Fluids, 2016, 28(2): 024105.

[23] Tian B, Zeng J, Meng B, Chen Q, Guo X, Xue K. Compressible multiphase particle-in-cell method (CMP-PIC) for full pattern flows of gas-particle system[J]. Journal of Computational Physics, 2020, 418: 109602.
[24] Zhou R, Meng B, Zeng J, Chen Q, Tian B. Numerical simulation of compressible fluid-particle flows in multimaterial Lagrangian hydrodynamics framework[J]. Computers & Fluids, 2021, 223: 104945.
[25] Si Y, Li S, Meng B, Wang C, Tian B. A dominant dimensionless number and theoretical model for the evolution of multiphase Richtmyer–Meshkov instability[J]. Physics of Fluids, 2024, 36(1): 013314.
[26] Shu C-W, Osher S. Efficient implementation of essentially non-oscillatory shock-capturing schemes, II[J]. Journal of Computational Physics, 1989, 83(1): 32–78.
[27] Harten A, Lax P D, Leer B van. On Upstream Differencing and Godunov-Type Schemes for Hyperbolic Conservation Laws[J]. Siam Review, 1983, 25: 53–79.
[28] Si Y, Li S, Chen Q, Meng B, Wang C, Tian B. Heat transfer effects on multiphase Richtmyer–Meshkov instability of dense gas–particle flow[J]. Physics of Fluids, 2023, 35(5): 053339.
[29] Meng B, Zeng J, Chen Q, Zhou R, Tian B. Numerical method for compressible gas-particle flow coupling using adaptive parcel refinement (APR) method on non-uniform mesh[J]. Journal of Computational Physics, 2022, 466: 111418.
[30] Reckinger S J, Livescu D, Vasilyev O V. Adaptive wavelet collocation method simulations of Rayleigh–Taylor instability[J]. Physica Scripta, 2010, T142: 014064.